Eur. Phys. J. C 49, 97–102 (2007)
DOI 10.1140/epjc/s10052-006-0062-0

THE EUROPEAN PHYSICAL JOURNAL C

Regular Article – Theoretical Physics

Space-time evolution of bulk QCD matter at RHIC

3D hydro + UrQMD model

C. Nonaka[1,a], S.A. Bass[2]

[1] Department of Physics, Nagoya University, Nagoya 464-8602, Japan
[2] Department of Physics, Duke University, Durham, NC 27708, USA

Received: 8 August 2006 /
Published online: 21 October 2006 –

Abstract. We introduce a combined fully three-dimensional macroscopic/microscopic transport approach employing relativistic 3D-hydrodynamics for the early, dense, deconfined stage of the reaction and a microscopic non-equilibrium model for the later hadronic stage where the equilibrium assumptions are not valid anymore. Within this approach we study the dynamics of hot, bulk QCD matter, which is being created in ultra-relativistic heavy-ion collisions at RHIC. In particular, we perform a detailed analysis of the reaction dynamics, hadronic freeze-out, transverse flow and elliptic flow.

PACS. 25.75.-q; 24.10.Nz; 24.10.Lx

1 Introduction

The first five years of RHIC operations at $\sqrt{s_{NN}} = 130$ GeV and $\sqrt{s_{NN}} = 200$ GeV have yielded a vast amount of interesting and sometimes surprising results [1], many of which have not yet been fully evaluated or understood by theory. There exists mounting evidence that RHIC has created a hot and dense state of deconfined QCD matter with properties similar to that of an ideal fluid [2] – this state of matter has been termed *strongly interacting quark–gluon plasma* (sQGP).

Relativistic fluid dynamics (RFD) is ideally suited for the *QGP and hydrodynamic expansion* reaction phase, but it breaks down in the later, dilute, stages of the reaction when the mean-free paths of the hadrons become large, and flavor degrees of freedom are important. The most important advantage of RFD is that it directly incorporates an equation of state as input and thus is so far the only dynamical model in which a phase transition can explicitly be incorporated. The hydrodynamic description has been very successful [3–5] in describing the collective behavior of soft particle production at RHIC.

Conventional RFD calculations need to assume a *freeze-out* temperature at which the hydrodynamic evolution is terminated and a transition from the zero mean-free-path approximation of a hydrodynamic approach to the infinite mean-free-path of free streaming particles takes place. The reach of RFD can be extended, and the problem of having to terminate the calculation at a fixed freeze-out temperature can be overcome by combining the RFD calculation with a microscopic hadronic cascade model – this kind of hybrid approach (dubbed *hydro plus micro*) was pioneered in [6] and has been now also taken up by other groups [7–9]. Its key advantages are that the freeze-out now occurs naturally as a result of the microscopic evolution and that flavor degrees of freedom are treated explicitly through the hadronic cross sections of the microscopic transport. Due to the Boltzmann equation being the basis of the microscopic calculation in the hadronic phase, viscous corrections for the hadronic phase are by default included in the approach.

Here, we combine the hydrodynamic approach with the microscopic ultra-relativistic quantum-molecular-dynamics (UrQMD) model [10, 11], in order to provide an improved description of the later, purely hadronic stages of the reaction (Fig. 1). We calculate the hadron distribution at switching temperature from the $3+1$ dimensional hydrodynamic model using the Cooper–Frye formula [12] and produce initial conditions for UrQMD model by Monte Carlo from it. Such hybrid macro/micro transport calcu-

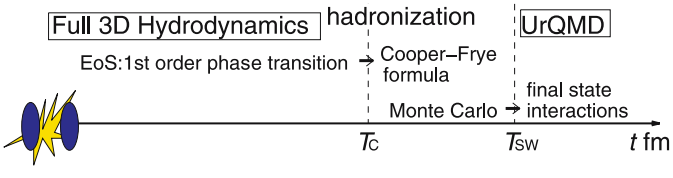

Fig. 1. Schematic sketch of 3D hydro + UrQMD model. T_c ($= 160$ MeV) and T_{sw} ($= 150$)MeV are critical temperature and switching temperature from hydrodynamics to UrQMD model, respectively

[a] email: nonaka@physics.umn.edu

lations are to date the most successful approaches for describing the soft physics at RHIC. The biggest advantage of the RFD part of the calculation is that it directly incorporates an equation of state as input – one of its largest limitations is that it requires thermalized initial conditions and one is not able to do an ab initio calculation.

2 Hydro + micro approach

2.1 Hydrodynamics

We shall use a fully three-dimensional hydrodynamic model [13] for the description of RHIC physics, especially focusing on Au + Au collisions at RHIC energies ($\sqrt{s_{NN}} = 200$ GeV per nucleon–nucleon pair). In hydrodynamic models, the starting point is the relativistic hydrodynamic equation

$$\partial_\mu T^{\mu\nu} = 0\,, \tag{1}$$

where $T^{\mu\nu}$ is the energy-momentum tensor which is given by

$$T^{\mu\nu} = (\epsilon + p)U^\mu U^\nu - p g^{\mu\nu}. \tag{2}$$

Here ϵ, p, U and $g^{\mu\nu}$ are energy density, pressure, four velocity and metric tensor, respectively. We solve the relativistic hydrodynamic equation (1) numerically with baryon number n_B conservation,

$$\partial_\mu \left(n_B(T,\mu)U^\mu\right) = 0\,. \tag{3}$$

In order to solve the relativistic hydrodynamic equations, we adopt Lagrangian hydrodynamics. In Lagrangian hydrodynamics, the coordinates of the individual cells do not remain fixed, but move along the flux of the fluid. In the absence of turbulence during the expansion, Lagrangian hydrodynamics has several advantages over the conventional Eulerian approach: they are computational expediency and analysis efficiency [14]. Our algorithm for solving the relativistic hydrodynamic equation in 3D is based on the conservation laws for entropy and baryon number. Further details concerning the numerical method can be found in [13].

To solve the relativistic hydrodynamic equation, an equation of state (EoS) needs to be specified. For the calculation presented in this work, we use a simple equation of state with the first order phase transition, which will allow us to compare our results to previous hydrodynamic and hybrid calculations employing $(1+1)$ dimensional [6] and $(2+1)$ dimensional [7, 8] hydrodynamic models.

Above the critical temperature ($T_c = 160$ MeV at $\mu = 0$ MeV), the thermodynamical quantities are assumed to be determined by the QGP gas which is dominated by massless u, d, s quarks and gluons. In the hadron gas below the critical temperature, the pressure for fermions is given by an excluded volume model [15]. In the low-temperature region the well-established (strange and non-strange) hadrons up to masses of ~ 2 GeV are included in the EoS [14]. Although heavy states are rare in a thermodynamical equilibrium, they have a larger entropy per particle than light states, and therefore have considerable impact on the evolution. In particular, hadronization is significantly faster as compared to the case where the hadron gas consists of light mesons only.

The actual model used for the hadronic stage of the reaction (UrQMD [10, 11]) additionally assumes a continuum of color-singlet states called "strings" above the $m \simeq 2$ GeV threshold to model $2 \to n$ processes and inelastic processes at high CM energy. For example, the annihilation of an $\overline{p}$ on an Ω is described as excitation of two strings with the same quantum numbers as the incoming hadrons, respectively, which are subsequently mapped on known hadronic states according to a fragmentation scheme. Since we shall be interested in the dynamics of the Ω-baryons emerging from the hadronization of the QGP, it is unavoidable to treat string formation. The fact that string degrees of freedom are not taken into account in the EoS of QGP phase does not represent a problem in our case since we focus on rapidly expanding systems where those degrees of freedom can not equilibrate [16].

The phase coexistence region is constructed employing Gibbs' conditions of phase equilibrium. The bag parameter of $B = 385$ MeV/fm^3 is chosen to yield the critical temperature $T_c = 160$ MeV at $\mu = 0$. At the coexistence phase of the QGP phase and the hadron phase we introduce the fraction of the volume of the QGP phase, $\lambda(x_\mu)$ $(0 \le \lambda \le 1)$ and parameterize the energy density and baryon number density [14].

The initial conditions for the hydrodynamic calculation need to be determined either by adjusting an appropriate parametrization to the data or by utilizing other microscopic transport model predictions for the early non-equilibrium phase of the heavy-ion reaction.

For our calculation we use a simple initial condition which is parameterized based on a combination of wounded nucleon and binary collision scaling [17–19]. We factorize the energy density and baryon number density distributions into longitudinal direction ($H(\eta)$) and the transverse plane ($W(x,y;b)$), which are given by

$$\begin{aligned} \epsilon(x,y,\eta) &= \epsilon_{\max} W(x,y;b) H(\eta)\,, \\ n_B(x,y,\eta) &= n_{B\max} W(x,y;b) H(\eta)\,, \end{aligned} \tag{4}$$

where $\epsilon_{\max}$ and $n_{B\max}$ are parameters which are the maximum values of the energy density and baryon number density. The longitudinal distribution is parameterized by

$$H(\eta) = \exp\left[-(|\eta| - \eta_0)/2\sigma_\eta^2\right] \theta(|\eta| - \eta_0)\,, \tag{5}$$

where the parameters η_0 and σ_η are determined by comparison with the experimental data of single particle distributions. The function $W(x,y;b)$ on the transverse plane is determined by the superposition of wounded nucleon scaling which is characteristic of "soft" particle production processes and binary collision scaling which is characteristic of "hard" particle production processes [20]. This function is normalized by $W(0,0;0)$. We set the initial longitudinal flow to Bjorken's scaling solution [21] and neglect

initial transverse flow. This is the simplest initial flow profile which will serve as basis for further investigation.

The parameters with which we reproduce single particle spectra at RHIC are $\tau_0 = 0.6\,\mathrm{fm}$, $\epsilon_{\max} = 40\,\mathrm{GeV/fm^3}$, $n_{B\max} = 0.15\,\mathrm{fm}^{-3}$, $\eta_0 = 0.5$ and $\sigma_\eta = 1.5$. The parameters η_0 and σ_η in longitudinal direction are determined mainly by the hadron rapidity distributions and do not strongly affect the transverse momentum distributions. In [14] we discussed the difference between initial condition of pure the hydrodynamic model and that of the hydro + UrQMD model in detail.

2.2 Results

Figure 2 shows the P_T spectra of π^+, K and p at $\sqrt{s_{NN}} = 200\,\mathrm{GeV}$ central collisions. The most compelling feature, compared to the pure 3D RFD calculation, is that the hydro + micro approach is capable of accounting for the proper normalization of the spectra for all hadron species without any additional correction as is performed in the pure hydrodynamic model. The introduction of a realistic freeze-out process provides, therefore, a natural solution to the problem of separating chemical and kinetic freeze-out in a pure hydrodynamic approach.

In Fig. 3 the centrality dependence of the P_T spectra of π^+ is shown. The impact parameter for each centrality is determined in the same way as in the pure hydrodynamic calculation. The separation between model results and experiment appears at lower transverse momentum in peripheral collisions compared to central collisions. The 3D hydro + micro model does not provide any improvement for this behavior, since the hard physics high P_T contribution to the spectra occurs at early reaction times before the system has reached the QGP phase and is therefore neither included in the pure 3D RFD calculation nor in the hydro + micro approach.

Figure 4 shows the centrality dependence of the pseudorapidity distribution of charged hadrons compared to PHOBOS data [23]. Solid circles stand for model results and open circles denote data taken by the PHOBOS collaboration [23]. The impact parameters are set to $b =$ 2.4, 4.5, 6.3, 7.9 fm for 0%–6%, 6%–15%, 15%–25% and 25%–35% centralities, respectively. Our results are consistent with experimental data over a wide pseudorapidity region. We observe a small deviation around $|\eta| \sim 3$, which may be improved by tuning the parameter σ_η (here we have chosen the same value as for the pure RFD calculation). There is no distinct difference between 3D ideal RFD model and the hydro + UrQMD model in the centrality dependence of the pseudorapidity distribution, indicating that the shape of the pseudorapidity distribution is insensitive to the detailed microscopic reaction dynamics of the hadronic final state.

In Fig. 5 we analyze the P_T spectra of multistrange particles. Our results show good agreement with experimental data for Λ, Ξ, Ω for centralities 0%–5%. In this calculation the additional procedure for normalization is not needed. Recent experimental results suggest that at thermal freeze-out multistrange baryons exhibit less transverse flow and a higher temperature, closer to the chem-

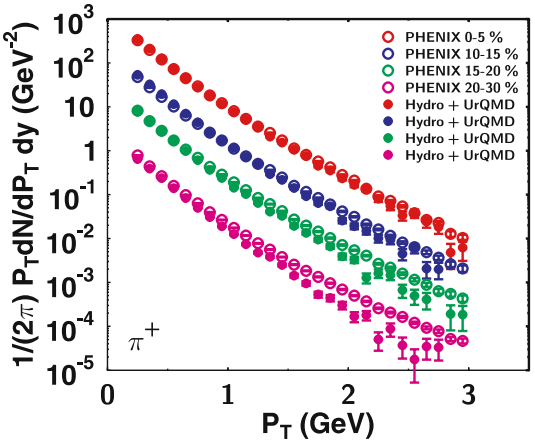

Fig. 3. Centrality dependence of P_T spectra of π^+ with PHENIX data [22]. The P_T spectra at 10%–15%, 15%–20% and 20%–30% are divided by 5, 25 and 200, respectively

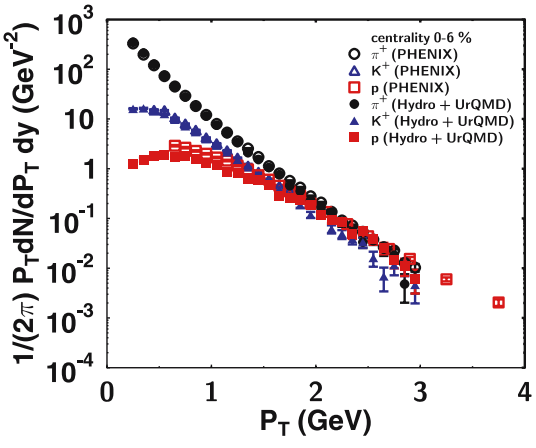

Fig. 2. P_T spectra for π^+, K^+ and p at central collisions with PHENIX data [22]. The *points* are not renormalized

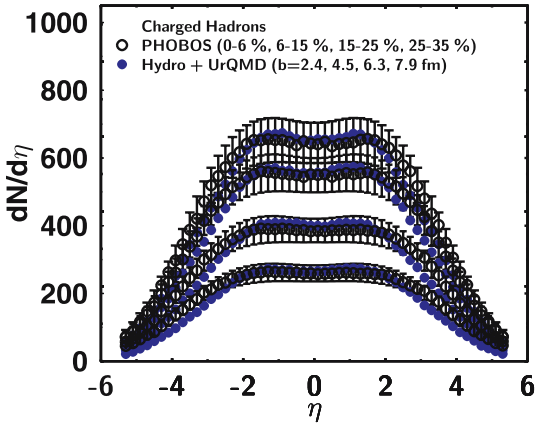

Fig. 4. Centrality dependence of pseudorapidity distribution of charged particles with the PHOBOS data [23]. The impact parameters in the calculation are 2.4 (0%–6%), 4.5 (6%–10%), 6.3 (10%–15%), 7.5 fm (25%–35%)

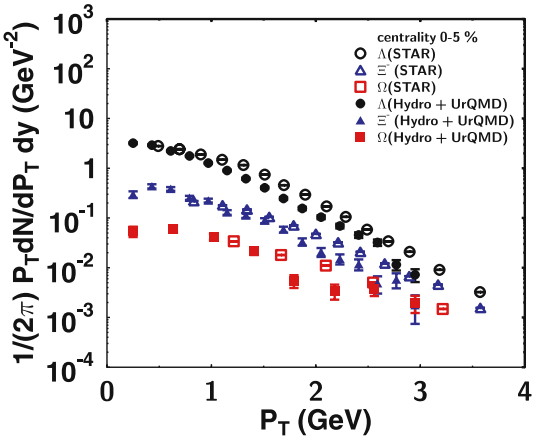

Fig. 5. $P_{\rm T}$ spectra of multi-strange particles at centralities 0%–5% and 10%–20% with the STAR data [24]

ical freeze-out temperature compared to non- or single-strange baryons [24, 25]. This behavior can be understood in terms of the flavor dependence of the hadronic cross section, which decreases with increasing strangeness content of the hadron. The reduced cross section of multi-strange baryons leads to a decoupling from the hadronic medium at an earlier stage of the reaction, allowing them to provide information on the properties of the hadronizing QGP less distorted by hadronic final state interactions.

In Fig. 6 the mean transverse momentum $\langle P_{\rm T}\rangle$ as a function of the hadron mass is shown. Open symbols denote the value at $T_{\rm sw} = 150\,{\rm MeV}$, corrected for hadronic decays. Not surprisingly, in this case the $\langle P_{\rm T}\rangle$ follows a straight line, suggesting a hydrodynamic expansion. However if hadronic rescattering is taken into account (solid circles) the $\langle P_{\rm T}\rangle$ do not follow the straight line anymore: the $\langle P_{\rm T}\rangle$ of pions is actually reduced by hadronic rescattering (they act as a heat-bath in the collective expansion), whereas protons actually pick up additional transverse momentum in the hadronic phase. RHIC data by the STAR collaboration is shown via the solid triangles – overall the proper treatment of hadronic final state interactions significantly improves the agreement of the model calculation with the data.

Let us now investigate the effect of resonance decays and hadronic rescattering on the pion and baryon transverse momentum spectra. Figure 7 shows the $P_{\rm T}$ spectrum for π^+ at $T_{\rm sw} = 150\,{\rm MeV}$ (solid line, uncorrected for resonance decays) as well as the final spectrum after hadronic rescattering and resonance decays, labeled as *hydro + UrQMD* (solid symbols). In addition the open symbols denote a calculation with the resonance decay correction performed at $T_{\rm sw}$, which we label as *hydro + decay*. The difference between the solid line and open symbols therefore directly quantifies the effect of resonance decays on the spectrum, which is most dominant in the low transverse momentum region $P_{\rm T} < 1\,{\rm GeV}$ Furthermore, the comparison between open symbols and solid symbols quantifies the effect of hadronic rescattering: pions with $P_{\rm T} > 1\,{\rm GeV}$ lose momentum via these final state interactions, resulting in a steeper slope.

Figure 8 shows a likewise analysis for baryons (p, Λ, Ξ and Ω). We note that in contrast to SPS energies [6], there is very little effect on the spectra due to hadronic rescattering – even for protons which rescatter 8–10 times at mid-rapidity. Only at low transverse momenta the multiple scattering of the protons (predominantly with pions) manifests itself in a slight flattening of the $P_{\rm T}$ distribution of the protons, giving rise to a slight increase in their radial flow. This phenomenon has been discussed in [6] and is commonly referred to as 'pion wind'.

Finally, let us move to the analysis of elliptic flow in the hydro + micro approach: first we show the elliptic flow coefficient v_2 as a function of $P_{\rm T}$ for π^+ at centralities 5%–10% and 10%–20% in Fig. 9. Open symbols stand for experimental data and solid symbols represent our calculations. We find that the hydro + micro approach is able to provide an improved agreement to the data compared to the purely hydrodynamic calculation [14].

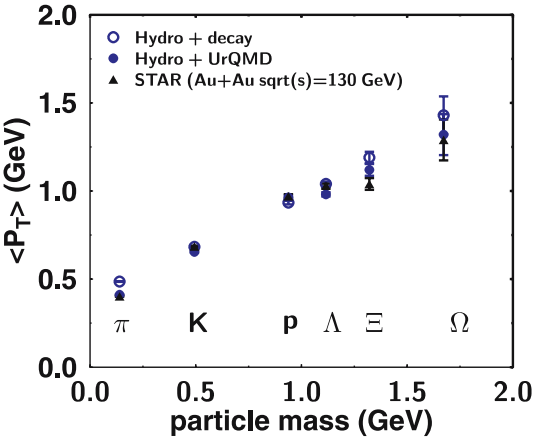

Fig. 6. Mean $P_{\rm T}$ as a function of mass. *Open circle symbols* stand for hydro + decay, *solid circle symbols* stand for hydro + UrQMD, and *solid triangle* stand for the STAR data (Au + Au $\sqrt{s_{\rm NN}} = 130\,{\rm GeV}$) [25]

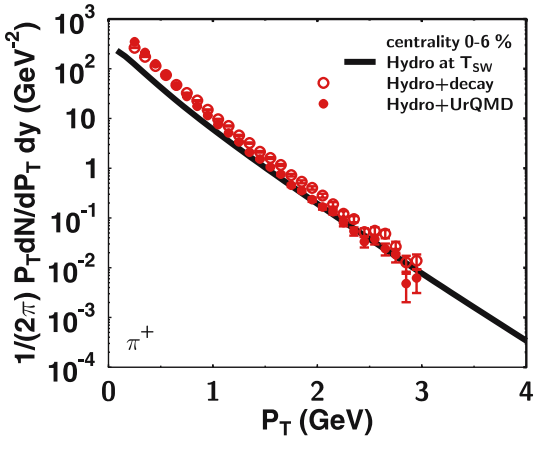

Fig. 7. $P_{\rm T}$ spectra of π^+ from hydro at switching temperature (*solid line*), hydro + decay (*open symbols*) and hydro + UrQMD (*solid symbols*) at central collision

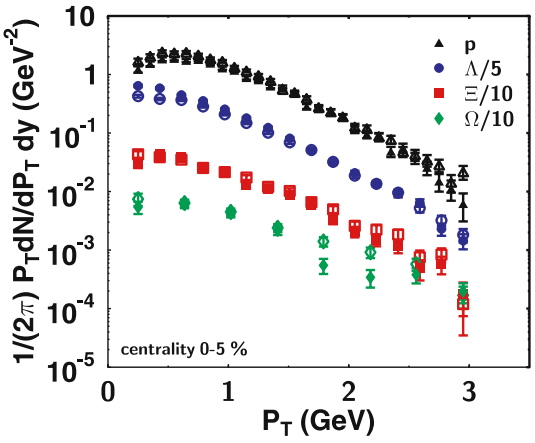

Fig. 8. $P_{\rm T}$ spectra of baryons from hydro + decay (*open symbols*) and hydro + UrQMD (*solid symbols*) at centrality 0%–5%

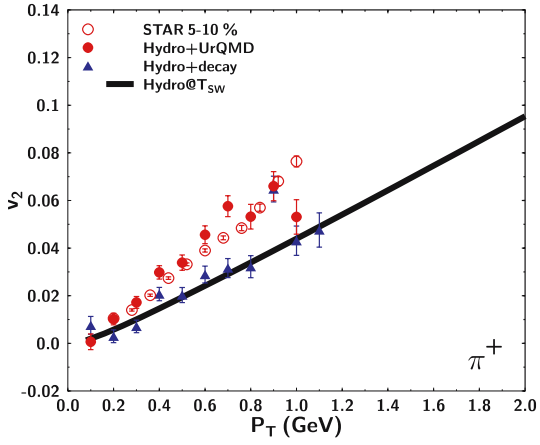

Fig. 10. Elliptic flow as a function of $P_{\rm T}$ of π^+ at centrality 5%–10% from pure hydro at the switching temperature (*solid line*), hydro + decay (*solid triangles*) and hydro + UrQMD (*solid circles*). *Open symbols* stand for the experimental data from STAR

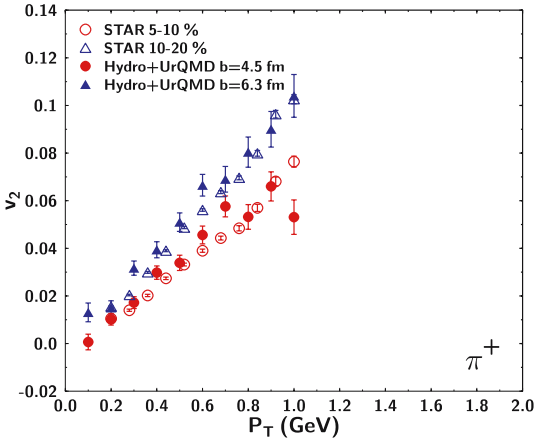

Fig. 9. Elliptic flow as a function of $P_{\rm T}$ for π^+ at centralities 5%–10% and 10%–20%. *Open symbols* stand for the STAR data [26] and *solid symbols* stand for our results

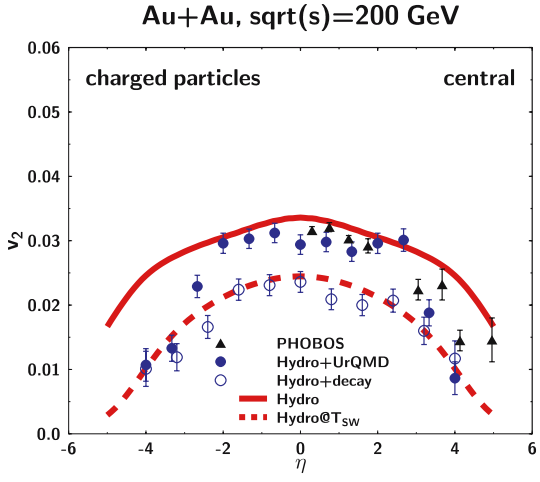

Fig. 11. Elliptic flow as a function of η of charged particles. *Solid line* and *dashed lines* stand for pure hydro calculation at the freeze-out temperature (110 MeV) and the switching temperature, respectively. Experimental data by PHOBOS are shown with *solid triangles* [30]. *Open* (*solid*) *circles* stand for hydro + decay (hydro + UrQMD)

The question of how much elliptic flow develops during the deconfined phase versus the hadronic phase is investigated in Figs. 10 and 11. It has been pointed out repeatedly, both in the framework of a microscopic [27] as well as a hydrodynamic analysis [18] that elliptic flow develops early on during the deconfined phase of the reaction and thus serves as a sensitive tool to study the equation of state of QCD matter. This picture has been confirmed by the experimentally observed quark number scaling $v_2^h \sim nv_2(1/nP_{\rm T})$ of elliptic flow at intermediate transverse momenta $P_{\rm T}$ [28, 29].

In Fig. 10 we plot the elliptic flow v_2 as a function of $P_{\rm T}$. The solid line stands for the pure hydro calculation, terminated at the switching temperature $T_{\rm sw}$ and solid circles denote the full hydro + micro calculation. We find that the QGP contribution to the elliptic flow depends on the transverse momentum – for low $P_{\rm T}$ nearly 100% of the elliptic flow is created in the QGP phase of the reaction, whereas the hadronic phase contribution increases to 25% at a $P_{\rm T}$ of 1 GeV/c.

Figure 11 shows the elliptic flow as a function of η: the pure hydrodynamic calculation is shown by the solid curve, the hydrodynamic contribution at $T_{\rm sw}$ is denoted by the dashed line and the full hydro + micro calculation is given by the solid circles, together with PHOBOS data (solid triangles). The shape of the elliptic flow in the pure hydrodynamic calculation at $T_{\rm sw}$ is quite different from that of the full hydrodynamic one terminated at a freeze-out temperature of 110 MeV. Apparently the slight bump at forward and backward rapidities observed in the full hydrodynamic calculation develops first in the later hadronic phase, since it is not observed in the calculation terminated at $T_{\rm sw}$. Evolving the hadronic phase in the hydro + micro approach will increase the elliptic flow at central rapidi-

ties, but not in the projectile and target rapidity domains. As a result, the elliptic flow calculation in the hydro + micro approach is closer to the experimental data when compared to the pure hydrodynamic calculation.

3 Summary

In summary, we have introduced a hybrid macroscopic/ microscopic transport approach, combining a newly developed relativistic $3+1$ dimensional hydrodynamic model for the early deconfined stage of the reaction and the hadronization process with a microscopic non-equilibrium model for the later hadronic stage at which the hydrodynamic equilibrium assumptions are not valid anymore. Within this approach we have dynamically calculated the freeze-out of the hadronic system, accounting for the collective flow on the hadronization hypersurface generated by the QGP expansion. We have compared the results of our hybrid model and of a calculation utilizing our hydrodynamic model for the full evolution of the reaction to experimental data. This comparison has allowed us to quantify the strength of dissipative effects prevalent in the later hadronic phase of the reaction, which cannot be properly treated in the framework of ideal hydrodynamics.

Overall, the improved treatment of the hadronic phase provides a far better agreement between the transport calculation and data, in particular concerning the flavor dependence of radial flow observables and the collective behavior of matter at forward/backward rapidities. We find that the hadronic phase of the heavy-ion reaction at top RHIC energy is of significant duration (at least $10\,\mathrm{fm}/c$) and that hadronic freeze-out is a continuous process, strongly depending on hadron flavor and momenta.

With this work we have established a base-line – both for the regular $3+1$ dimensional hydrodynamic model as well as for the hybrid hydro + micro approach. In forthcoming publications we shall expand on this base-line by investigating the effects of a realistic lattice-QCD motivated equation of state containing a tri-critical point [31] and by performing an analysis of two particle correlations (HBT interferometry). We also plan to use our model as the medium for the propagation of jets and heavy quarks and to study the modification of our medium due to the passage of these hard probes.

References

1. 'First Three years of Operation of RHIC', Nucl. Phys. A **757**, Procedings at 18th International Conference on 'Nucleus–Nucleus Collision' (Quark Matter 2005)
2. 'Quark–Gluon Plasma', Nucl. Phys. A **757**
3. P.F. Kolb, U.W. Heinz, arXiv:nucl-th/0305084
4. P. Huovinen, arXiv:nucl-th/0305064
5. T. Hirano, K. Tsuda, Phys. Rev. C **66**, 054 905 (2002)
6. S.A. Bass, A. Dumitru, Phys. Rev. C **61**, 064 909 (2000)
7. D. Teaney, J. Lauret, E.V. Shuryak, Phys. Rev. Lett. **86**, 4783 (2003)
8. D. Teaney, J. Lauret, E.V. Shuryak, nucl-th/011037
9. T. Hirano, U.W. Heinz, D. Kharzeev, R. Lacey, Y. Nara, Phys. Lett. B **636**, 299 (2006)
10. S.A. Bass et al., Progr. Part. Nucl. Physics **41**, 225 (1998)
11. M. Bleicher et al., J. Phys. G **25**, 1859 (1999)
12. F. Cooper, G. Frye, Phys. Rev. D **10**, 186 (1974)
13. C. Nonaka, E. Honda, S. Muroya, Eur. Phys. J. C **17**, 663 (2000)
14. C. Nonaka, S.A. Bass, nucl-th/0607018
15. D.H. Rischke et al., Z. Phys. C **51**, (1991)
16. M. Belkacem et al., Phys. Rev. C **58**, 1727 (1998)
17. P. Jacobs, G. Cooper, nucl-ex/0008015
18. P.F. Kolb, J. Sollfrank, U. Heinz, Phys. Rev. C **62**, 054 909 (2000)
19. P.F. Kolb et al., Nucl. Phys. A **696**, 197 (2001)
20. U. Heinz, P.F. Kolb, Phys. Lett. B **542**, 216 (2002)
21. J.D. Bjorken, Phys. Rev. D **27**, 140 (1983)
22. PHENIX Collaboration, S.S. Adler et al., Phys. Rev. C **69**, 034 909 (2004)
23. PHOBOS Collaboration, B.B. Back et al., Phys. Rev. Lett. **91**, 052 303 (2003)
24. M. Estienne (for the STAR Collaboration), J. Phys. G **31**, 873 (2005)
25. STAR Collaboration, J. Adames et al., Phys. Rev. Lett. **92**, 182 301 (2004)
26. STAR Collaboration, J. Adams et al., Phys. Rev. C **72**, 014 904 (2005)
27. H. Sorge, Phys. Rev. Lett. **78**, 2309 (1997)
28. STAR Collaboration, J. Adams et al., Phys. Rev. Lett. **92**, 052 302 (2004)
29. D. Molnar, S.A. Voloshin, Phys. Rev. Lett. **91**, 092 301 (2003)
30. PHOBOS Collaboration, B.B. Back et al., Phys. Rev. C **72**, 051 901(R) (2005)
31. C. Nonaka, M. Asakawa, Phys. Rev. C **71**, 044 904 (2005)